Journal of Materials Chemistry A

Accepted Manuscript

ROYAL SOCIETY OF CHEMISTRY

www.rsc.org/materialsA

Encapsulating $Ca_2Ge_7O_{16}$ nanowires within graphene sheets as anode materials for lithium-ion batteries

Wenwu Li, Di Chen* and Guozhen Shen*

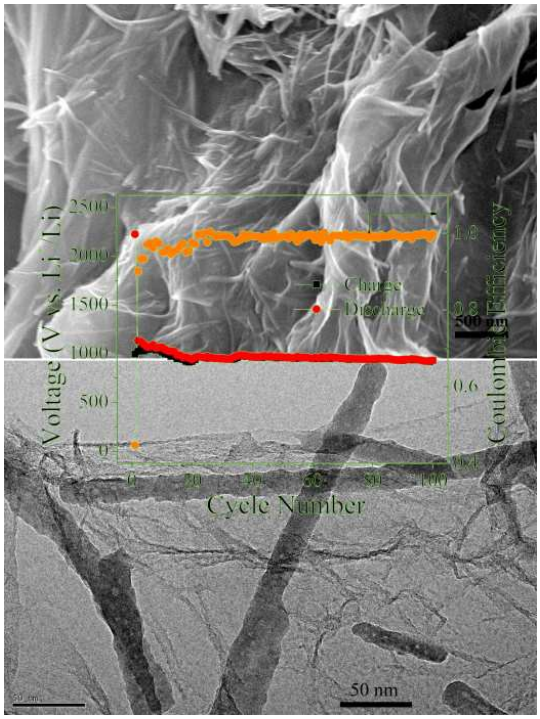

Single-crystal $Ca_2Ge_7O_{16}$ nanowires encapsulated within graphene sheets exhibit high specific capacity, good cyclability, and excellent rate capability for anodes of lithium ion batteries.

Cite this: DOI: 10.1039/c0xx00000x

www.rsc.org/xxxxxx

ARTICLE TYPE

Encapsulating $Ca_2Ge_7O_{16}$ nanowires within graphene sheets as anode materials for lithium-ion batteries

Wenwu Li[a,b], Di Chen[a]* and Guozhen Shen[c]*

Received (in XXX, XXX) Xth XXXXXXXXX 200X, Accepted Xth XXXXXXXXX 200X

DOI: 10.1039/b000000x

Single-crystal $Ca_2Ge_7O_{16}$ nanowires (~ 10 nm in diamter) have been encapsulated within graphene sheets successfully to form nanocomposite with three-dimensional hierarchical nanostructures by a facile hydrothermal method on a large scale. The as-synthesized $Ca_2Ge_7O_{16}$ nanowires/graphene sheets nanocomposite electrode exhibits high specific capacity (ca. 950 mA h g^{-1} at the current density of 100 mA g^{-1}), good cyclability, and excellent rate capability (ca. 400 mA h g^{-1} at the current density of 3200 mA g^{-1}). Such superior lithium storage performance, on the one hand, could be assigned to the graphene sheets which act as conductive substrates and elastic networks to disperse and encapsulate the $Ca_2Ge_7O_{16}$ nanowires, thereby effectively relieving the volume changes and aggregation of the nanoparticles during the Li^+ insertion/extraction. And on the other hand, the synergistic effect of the unique nanostructured hybrid, in which the $Ca_2Ge_7O_{16}$ nanowires are well-stabilized by graphene sheets with high conductivity and flexibility, is beneficial to enlarge the specific surface area, deliver enough sites to allow dispersion of the Ge nanoparticles, and provide void space to buffer the volume change during discharge/charge cycles. The work provides an effective strategy for the fabrication of functionalized ternary-oxide-based composites as high-performance electrode materials that involve poor conductivity and severe electrode pulverization.

Introduction

There is an urgent requirement to develop rechargeable lithium ion batteries (LIBs) with high energy density and power density for application in hybrid electric vehicles and electric vehicles.[1-7] However, commercial graphite anode used currently has already reached its theoretical limit (372 mA h g^{-1}), and thus exploring alternative anode materials with higher capacity, cyclability and rate capability has become an urgent task nowadays. In this context, germanium (1600 mA h g^{-1}) has been extensively exploited as anode materials for high-performance LIBs due to intrinsic merits such as faster Li^+ (400 times for germanium) and electron (4 magnitude order for germanium) transport than silicon.[8-22] However, pure element Ge anodes suffer from rapid capacity loss due to agglomerations resulting in increased diffusion lengths as well as structural pulverization caused by the large volume changes and consequent local strain generated during the Li^+ insertion/extraction.[23-24] In contrast, investigations of ternary oxides as anode materials are relatively scarce. In particular, ternary-oxide materials are technologically important because of their more complex functions and intriguing properties, which are readily tunable by adjusting the ratio of the dopant or alloying components.[25-28] In terms of the ternary germanates, the extra *in-situ* formed metal, metal oxide and Li_2O mixture matrix during first several discharge/charge cycles, can not only disperse uniformly Ge nanoparticles to adjust effectively the variation of volume, also catalyze the reaction: Ge→GeO_2 to improve the capacity dramatically.[26-30] Till now, several nanostructured ternary oxides (e.g. $ZnCo_2O_4$, Zn_2GeO_4, $CuGeO_3$, etc) have been reported in lithium storage. Even so, the synthesis and design of ternary oxides with high performance still remain full of challenges. By comparison, $Ca_2Ge_7O_{16}$ not only obtains facile preparation in a large scale, low-cost, environmental benign, and good stabilized matrix but also can deliver large lithium storage capacity with a low and non-stepped plateau which is beneficial to achieve the applied high energy density for full batteries. Therefore, much attention has been paid to $Ca_2Ge_7O_{16}$ as anode material for LIBs.[6, 25, 31-32] However, they just investigated its inherent lithium storage performances with different morphologies. The poor conductivity severely limits its electrochemical performances and therefore, further modified $Ca_2Ge_7O_{16}$ to effectively promote the electronic conductivity is badly in need of solution.

Recently, the increasing attention has been focused on graphene, a novel two-dimensional carbon matrix to replace other carbon matrices (e.g. graphite, CNT, etc) for supporting metal and metal oxides to form functional nanocomposite owing to its excellent properties such as high conductivity, unique mechanical properties and large specific surface areas. And graphene-based or graphene-encapsulated inorganic materials show excellent electrochemical lithium storage performance for LIBs.[33-37] The enhanced electrochemical lithium storage performance can be assigned to the graphene substrate, because it can improve the

electronic conductivity of the overall electrode, benefit the high dispersion of nanomaterials, and effectively buffer the strain from the volume variation during lithiation and delithiation processes.

Herein, we report a new preparation process for three-dimensional hierarchical architectures constructed of single-crystal $Ca_2Ge_7O_{16}$ nanowires/graphene sheets through a facile one-step method, without the addition of any surfactants. When evaluated as an anode material for LIBs, the resulting $Ca_2Ge_7O_{16}$/graphene nanocomposite exhibits greatly improved specific capacity, cyclability, and rate capability in comparison to the pristine $Ca_2Ge_7O_{16}$ nanowires. The $Ca_2Ge_7O_{16}$/graphene nanocomposite delivers a highly reversible capacity of ca. 950 mA h g^{-1} over 100 cycles between 0 and 3 V at a current density of 100 mA g^{-1}. What is more, a highly reversible capacity of 400 mA h g^{-1} can still be obtained at the current density of 3200 mA g^{-1}. And this work provides an effective strategy for the synthesis of functionalized ternary-oxide-based composites in an *in-situ* way to apply in various fields.

Experimental

Materials: Graphene was purchased from Nanjing XFNano Material Tech Co., Ltd., and its thickness was about 0.8 nm. All other reagents were analytically pure and used without further purification. Synthesis of $Ca_2Ge_7O_{16}$ nanowires/graphene nanocomposite: in a typical experiment, graphene (50 mg) was dispersed into distilled water (35 mL) under magnetic stirring and sonication for 100 min and after that, 0.5 mmol calcium acetate and 1.75 mmol GeO_2 were dissolved. After stirred for ca. 30 min, the solution was transferred into a Teflon-lined stainless steel autoclave with a capacity of 50 mL for hydrothermal treatment at 180 °C for 8 h. The autoclave was cooled to room temperature naturally, and then the precipitates were separated by centrifugation, washed with distilled water and absolute ethanol, and dried in a vacuum oven at 80 °C for 12 h.

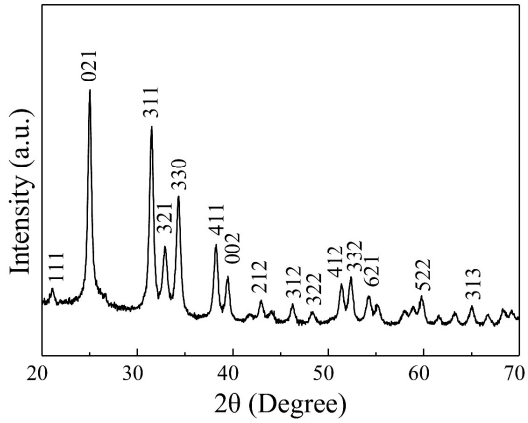

Figure 1. XRD pattern of the as-synthesized $Ca_2Ge_7O_{16}$/graphene sheets nanocomposite.

The crystal structures of the as-synthesized products were investigated by X-ray diffraction (XRD; X'Pert PRO, PANalytical B.V., the Netherlands) with radiation from a Cu target (K_α, λ = 0.15406 nm). The morphology and microstructure of the as-synthesized $Ca_2Ge_7O_{16}$/graphene hybrid were characterized by field-emission scanning electron microscopy (FESEM; JEOL JSM-6700F, 5 kV), and transmission electron microscopy (TEM; JEOL, JEM-2010 HT). XPS measurements were performed on a VG MultiLab 2000 system with a monochromatic $Al_{K\alpha}$ X-ray source (ThermoVG Scientific). TG analysis (DTA) was performed on a PerkinElmer Diamond TG/DTA apparatus at a heating rate of 10 °C/min in flowing air. Raman measurement was performed on a Bruker RAM II FT-Raman module that was coupled to the optical bench of a Bruker VERTEX 70 FTIR spectrometer.

The electrodes were prepared by mixing the active material, super P, and polyvinyldifluoride (PVDF, mass ratio 7:2:1) in *N*-methylpyrrolidone to form a slurry. The slurry was pasted onto copper foil and dried under vacuum at 80 °C for 24 h. Then, it was cut into round pieces with a diameter of 8 mm. The 2032 coin cells were assembled in a glove box filled with argon gas. Lithium metal was used as the counter electrode; a mixture of ethylene carbonate and diethyl carbonate (EC/DEC, 1:1 v/v) that contained 1 M $LiPF_6$ was used as the electrolyte. The galvanostatic discharge/charge tests were carried out by using the Land Battery measurement system (Wuhan, China) with a cutoff potential of 0-3 V *vs.* Li^+/Li. Cyclic voltammograms were measured at a scan rate of 0.1 mV s^{-1} on an electrochemical work station (CHI 660d).

Results and discussion

The synthetic process of $Ca_2Ge_7O_{16}$ nanowires/graphene sheets nanocomposite is schematically illustrated in **Scheme 1.** Firstly, free Ca^{2+} ions which derived from calcium acetate, were adhered onto the surface of graphene sheets through electrostatic interaction, and meanwhile GeO_2 reacted with OH^-, which came from the hydrolysis of CH_3COO^-, forming into $HGeO_3^-$. When the concentrations of the $HGeO_3^-$ and Ca^{2+} ions reach the supersaturation limit, small $Ca_2Ge_7O_{16}$ nuclei are generated and anchored onto the surface of graphene sheets, which prevents the restacking of graphene sheets. With increasing reaction time, the $Ca_2Ge_7O_{16}$ experienced a Ostwald ripening process to grow into nanowires forming into a sandwich-like structure with graphene sheets.

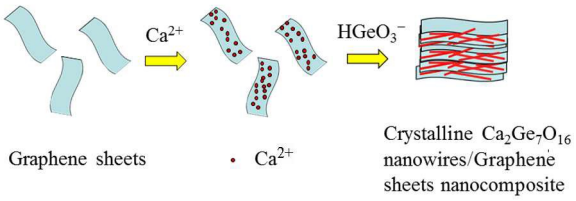

Scheme 1. Synthetic route to $Ca_2Ge_7O_{16}$ nanowires/graphene sheets nanocomposite.

The crystalline structure of the $Ca_2Ge_7O_{16}$/graphene sheets nanocomposite was characterized by X-ray diffraction (XRD). As shown in **Figure 1**, all of the diffraction peaks can be well indexed to the orthorhombic phase of $Ca_2Ge_7O_{16}$ (JCPDS Card No. 34-0286). No obvious peaks assigned to carbon are found in the XRD pattern, thus indicating that the carbon in the $Ca_2Ge_7O_{16}$/ graphene sheets product is not well-crystallized.

The existence of carbon in the $Ca_2Ge_7O_{16}$/graphene sheets composite was confirmed by Raman spectroscopy. As shown in **Figure 2a**, the characteristic D band and G band are observed at 1294 cm^{-1} and 1596 cm^{-1}, respectively. The G band corresponds to the zone center E_2g mode, which is related to phonon vibrations in sp^2 carbon materials, and the D band is commonly assigned to a breathing mode of A_1g symmetry that involves phonons near the *K*-zone boundary.[38] X-ray photoelectron spectroscopy (XPS) was employed to analyze the information on the surface chemical compositions and the valence states of the $Ca_2Ge_7O_{16}$ nanowires/graphene sheets composite. From **Figure 2b**, it can be seen that the as-synthesized nanocomposite is composed of Ca, Ge, O, C species. And as shown in **Figure 2c**, the high-resolution XPS spectrum of C 1s centered at 284.9 eV corresponds to C_{sp2}-C_{sp2}. From **Figure 2d** together with Figure S1 (TG analysis of pure $Ca_2Ge_7O_{16}$),[32] we can see that the carbon content in the $Ca_2Ge_7O_{16}$/graphene sheets nanocomposite is evaluated to be ca. 14% by thermogravimetric analysis.

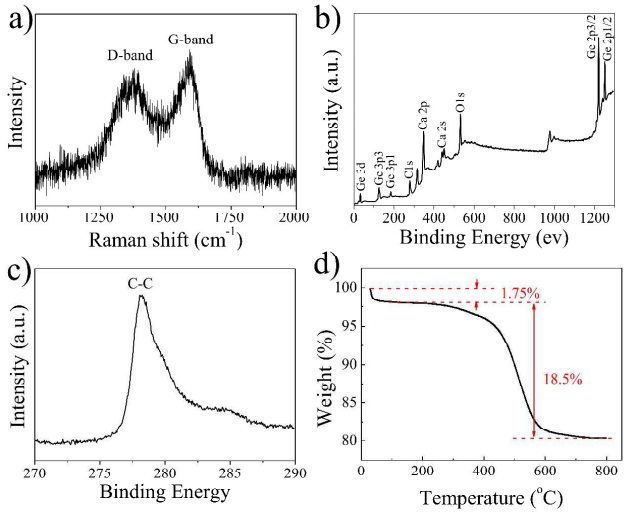

Figure 2. Raman, XPS spectra and TG of the $Ca_2Ge_7O_{16}$ nanowires/graphene sheets nanocomposite: a) Raman spectrum; b) survey XPS spectrum; c) high-resolution spectrum of C 1s; d) TG curve of the composites measured in the flowing air at a heating rate of 10 ºC min^{-1}.

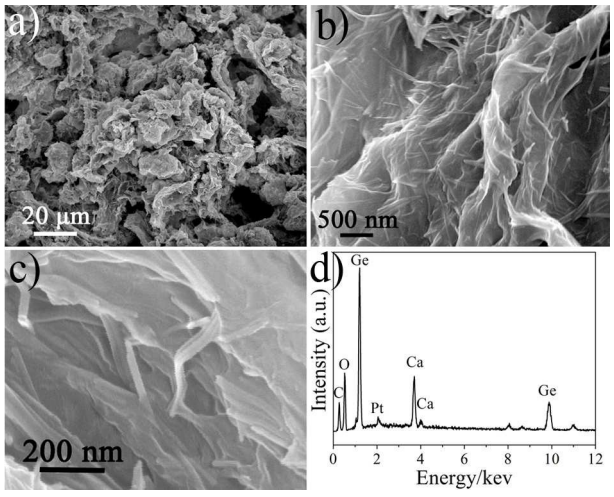

Figure 3. a-c) FESEM images and d) EDX spectrum of the $Ca_2Ge_7O_{16}$/graphene sheets nanocomposite.

The morphology of the products was examined by field-emission scanning electron microscopy (FESEM). **Figure 3a** is a typical FESEM image of the as-synthesized $Ca_2Ge_7O_{16}$/graphene sheets nanocomposite at low magnification. This image shows that the resulting nanocomposite is micrometer-sized and the surface is rough and wrinkled. **Figure 3b and c** show high-magnification SEM images that the wrinkled graphene sheets constructed a conductive network and well encapsulated the $Ca_2Ge_7O_{16}$ nanowires with an average diameter of ca. 10 nm and lengths within the range 1-2 μm. The elemental composition of the $Ca_2Ge_7O_{16}$/graphene sheets nanocomposite was further confirmed by energy-dispersive X-ray microanalysis, as shown in **Figure 3d**. The microanalysis confirms the presence of Ca, Ge, O, and C species, as well as signals of Pt, which was generated by Pt sputtering for decreasing the charging effects under the SEM-imaging conditions.

To get more information about microstructures of the as-synthesized products, transmission electron microscopy (TEM) and high-resolution TEM (HRTEM) characterizations were performed. **Figure 4a** shows a low-magnification TEM image of the $Ca_2Ge_7O_{16}$ nanowires/graphene sheets, which indicates that the obtained $Ca_2Ge_7O_{16}$ nanowires are encapsulated well within graphene sheets. **Figure 4b** shows a high-magnification image, which further demonstrates that the $Ca_2Ge_7O_{16}$ nanowires with ultrathin diameter (ca. 10 nm) are well wrapped into graphene sheets. The corresponding selected area electron diffraction (SAED) pattern is shown in **Figure 4c.** The SAED patterns of different nanowires or different positions on a given single nanowire are essentially identical, thus indicating that the $Ca_2Ge_7O_{16}$ nanowires are single crystals. The HRTEM image (**Figure 4d**) further confirms the microstructure of the $Ca_2Ge_7O_{16}$ nanowires/graphene sheets. The fringes are separated by ca. 0.359 nm, which agrees well with the (021) lattice spacing of the orthorhombic $Ca_2Ge_7O_{16}$. As for the growth direction of the $Ca_2Ge_7O_{16}$ nanowires within the graphene nanosheets, as shown in the screenshot (Figure S2) of Figure 4b and another HRTEM (Figure S3), we can conclude that $Ca_2Ge_7O_{16}$ nanowires within graphene sheets grow along the [001] direction. And the results are consistent with the previous reports.[6, 25]

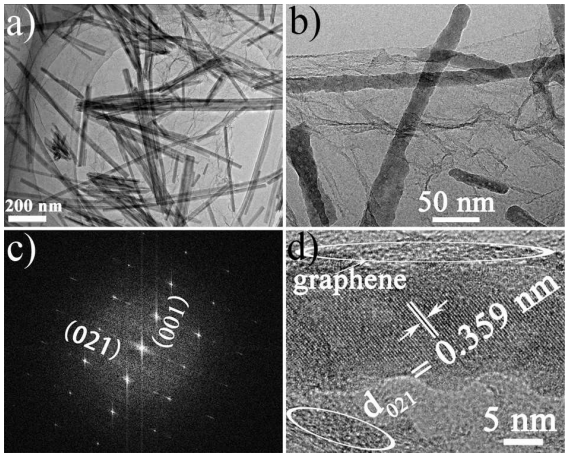

Figure 4. a, b) TEM images, c) selected-area electron diffraction (SAED) pattern, and d) HRTEM image of the $Ca_2Ge_7O_{16}$/graphene sheets nanocomposite.

The lithium-storage performance of the as-synthesized $Ca_2Ge_7O_{16}$/graphene sheets nanocomposite was investigated by cyclic voltammetry and by galvanostatic discharge/charge measurements. **Figure 5a** shows the CV curves of $Ca_2Ge_7O_{16}$ nanowires/graphene sheets nanocomposite based electrode at a scan rate of 0.1 mV s^{-1} within the potential range 0-3 V. Evidently, the first CV scan is substantially different from subsequent ones. Upon the initial cathodic sweep, reduction peaks between 2.5 V and 0.4 V may be attributed to the reduction of $Ca_2Ge_7O_{16}$ into CaO, Ge, and Li_2O, as well as the irreversible formation of solid electrolyte interface (SEI) reaction that is related to the decomposition of the electrolyte.[39] At lower potentials, the pronounced cathodic peaks between 0.4 and 0 V can be assigned to the alloy reactions of Li_xGe ($0<x\leq4.4$). In the subsequent cycles, the main cathodic peaks shift to 0.18 and 0.36 V, corresponding to the formation of the $Li_{4.4}Ge$ alloy by lithium insertion, thus distinguishing the later reduction mechanism from the first one. During the anodic potential sweeps, three broad oxidation peaks are observed, the first two, 0.38 and 0.5 V, which are associated with the delithiation of Li_xGe ($0<x\leq4.4$),[40] and the third, 1.25 V, followed by the partial oxidation of Ge.[41-43] Remarkably, the CV curves do not vary dramatically from the second cycle onward, suggesting a highly reversible lithium uptake and release once the initial structural changes are completed. In contrast, the CV curves (see Figure S4) of the pristine $Ca_2Ge_7O_{16}$ nanowires with onward instability do not show that broad peaks, which further indicate the merits of incorporation of graphene sheets. The overall electrochemical reaction process during Li insertion/extraction can be described as follows:[5, 26, 29-30, 41-43, 44-45]

$$Ca_2Ge_7O_{16} + 28\ Li^+ + 28\ e^- \rightarrow 7\ Ge + 2\ CaO + 14\ Li_2O \quad (1)$$

$$Ge + 4.4\ Li^+ + 4.4\ e^- \leftrightarrow Li_{4.4}Ge \quad (2)$$

$$Ge + 2\ Li_2O \leftrightarrow GeO_2 + 4\ Li^+ + 4\ e^- \quad (3)$$

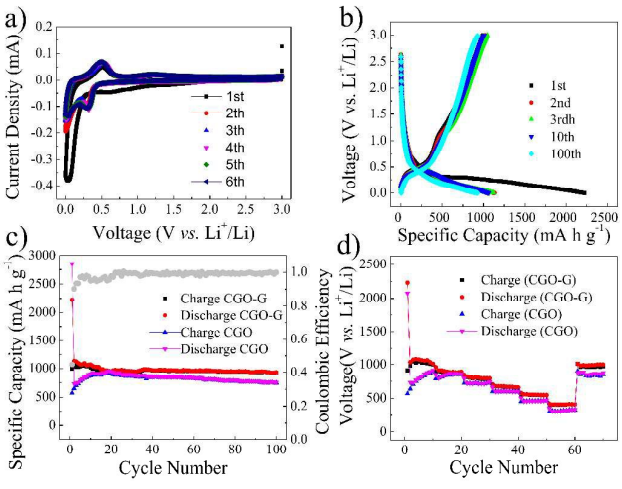

Figure 5. (a) Cyclic voltammetry curves within the potential window of 0-3 V (scan rate: 0.1 mV s^{-1}). (b) Typical voltage-specific capacity profiles for the first, second, third, 10th, and 100th discharge-charge cycles of the $Ca_2Ge_7O_{16}$ nanowires/graphene sheets nanocomposite. (c) Cycling performance and corresponding coulombic efficiency of the $Ca_2Ge_7O_{16}$ nanowires/graphene sheets nanocomposite (CGO-G) and cycling performance of the pristine $Ca_2Ge_7O_{16}$ nanowires (CGO) at the current density of 100 mA g^{-1} within the voltage range of 0-3 V. (d) Specific capacity-cycle number plot at increasing current densities from 0.1 A g^{-1} to 3.2 A g^{-1}.

Figure 5b depicts the first, second, third, 10th and 100th galvanostatic discharge/charge profiles for the as-prepared $Ca_2Ge_7O_{16}$ nanowires/graphene sheets nanocomposite that is cycled at the current density of 100 mA g^{-1} over the potential cutoff 0-3.0 V. The initial specific capacities for discharge and charge are as high as ca. 2200 and 1000 mA h g^{-1}, respectively. And the incomplete conversion reaction and irreversible lithium uptake due to the formation of SEI layer, similar phenomenon reported previously in metal-oxide anodes that were based on conversion- and alloy-type cycling mechanisms should be responsible for the capacity gap.[44-49] The initial coulombic efficiency of the $Ca_2Ge_7O_{16}$ nanowires/graphene sheets nanocomposite is ca. 45% which is much higher than that of pristine $Ca_2Ge_7O_{16}$ nanowires (ca. 18%, such a low initial coulombic efficiency (18.1%) has also been observed by Guo, et al.[4a]). The efficiency of the composite approaches quickly to almost 100% after several cycles and remains steady in subsequent cycles although the voltage window is expanded to 3.0 V. From the trend of the second, third, 10th, 100th discharge/charge curves, it can be seen that two distinct discharge voltage plateaus, ca. 0.18 and 0.36 V, correspond to the formation of $Li_{4.4}Ge$ alloy by lithium insertion and two main charge plateaus, ca. 0.38 and 0.5 V, correspond to the dealloy reaction.[40] These discharge/charge curves display the same trend, which are in good agreement with the above electrochemical results of CVs and also agree well with the previously reported results. Such low voltage plateaus *vs.* metal Li of the reversible alloying-dealloying reactions will contribute to the increase of output voltage of the full cell with the $Ca_2Ge_7O_{16}$ nanowires/graphene sheets anodes.

To emphasize the unprecedent electrochemical lithium storage performance of the $Ca_2Ge_7O_{16}$ nanowires/graphene sheets nanocomposite electrode, the pristine $Ca_2Ge_7O_{16}$ nanowires electrode that was directly prepared by hydrothermal methods without using graphene sheets was also prepared and its electrochemical performance was also performed. The XRD diffraction pattern of the bare $Ca_2Ge_7O_{16}$ nanowires can be well indexed to a pure phase of orthorhombic $Ca_2Ge_7O_{16}$ (Figure S5). The FESEM images (Figure S6) show pristine $Ca_2Ge_7O_{16}$ nanowires were tightly binded to each other to become thicker, which is detrimental to lithium insertion.

Figure 5c depicts the discharge-charge capacities *vs.* cycle number of the $Ca_2Ge_7O_{16}$ nanowires/graphene sheets nanocomposite electrode at the current density of 100 mA g^{-1}. It clearly reveals that, except for the irreversible capacity for the first discharge (ca. 2200 mA h g^{-1}), the following charge-discharge capacities in the regime of measurement appeared to be stable with specific capacity in the range of 950-1000 mA h g^{-1} and the coulombic efficiency is higher than 99% from the 20th to the 100th cycles (Figure 5c, gray solid cycles). Good capacity retention can be found for the $Ca_2Ge_7O_{16}$ nanowires/graphene sheets electrode and there is no obvious capacity loss up to 100 discharge/charge cycles, demonstrating highly reversible specific capacity and cyclability. Compared with the pristine $Ca_2Ge_7O_{16}$ nanowires (XRD in Figure S5 and SEM images in Figure S6)

electrode (the corresponding electrochemical data are also shown in Figure 5c), the three-dimensional, hierarchical $Ca_2Ge_7O_{16}$ nanowires/graphene sheets nanocomposite electrode shows much better lithium storage performance especially in cyclability and specific capacity. The specific capacity of pristine $Ca_2Ge_7O_{16}$ nanowires decays dramatically upon cycling at a current density of 100 mA g^{-1}. The pristine $Ca_2Ge_7O_{16}$ nanowires anode only delievers a specific capacity of below 700 mA h g^{-1} after 100 cycles. In addition, the resulting $Ca_2Ge_7O_{16}$ nanowires/graphene sheets nanocomposite in this work also exhibits higher capacity and better rate capability than previously reported $Ca_2Ge_7O_{16}$ nanowires electrode prepared through a hydrothermal process.

Apart from large reversible capacity and good cyclability, the rate capability is another essential characteristic for high-performance LIBs. **Figure 5d** further shows the rate performance of the $Ca_2Ge_7O_{16}$ nanowires/graphene sheets and of pristine $Ca_2Ge_7O_{16}$ nanowires anodes cycling at increasing current densities varying from 0.1 to 3.2 A g^{-1}, respectively. Obviously, the capacities of $Ca_2Ge_7O_{16}$ nanowires/graphene sheets nanocomposite were found to decrease from ca. 1000, 900, 750, 700 to 650 mA h g^{-1} with increasing current density varying from 0.1, 0.2, 0.4, 0.8, to 1.6 A g^{-1}, respectively. Even at the ultrahigh current density of 3.2 A g^{-1}, the $Ca_2Ge_7O_{16}$ nanowires/graphene sheets nanocomposite anodes can still maintain a relatively satisfactory specific capacity of ca. 400 mA h g^{-1}, much higher than the graphite theoretical capacity of ca. 372 mA h g^{-1}. The specific capacity is then bounced back to ca. 1000 mA h g^{-1} once the current density was resetted back to 0.1 A g^{-1}, revealing most of the initial capacity at the current density of 0.1 A g^{-1} was recovered. Besides, from those curves, we can also see that the cycling stability is quite excellent on each stage although the current density was increasing aggressively. However, in contrast, the pristine $Ca_2Ge_7O_{16}$ nanowires electrodes show inferior electrochemical lithium storage performance whether in terms of the specific capacity on each current stage or cyclability. It can be seen that clearly, in the control experiment, the pristine $Ca_2Ge_7O_{16}$ nanowires electrode can not bounce back to its initial specific capacity even though the current density was returned to the initial 100 mA g^{-1}.

Many previous pure Ge anode investigations fix the voltage window between 0 and 1.5 V.[8, 50] A wider cutoff window (0 and 3.0 V) was applied in this work, although the main electrochemical lithium storage reactions of the as-synthesized $Ca_2Ge_7O_{16}$ nanowires/graphene sheets occur below 1.3 V, which is similar to graphite and much lower than the nanosized conversion-type active materials. It is well-known that a wider cutoff window and larger constant current can be employed as harsher conditions to test the abilities of the electrodes and the performance of $Ca_2Ge_7O_{16}$ nanowires/graphene sheets as anode materials to use for LIBs and to demonstrate its advantages over the known conversion active materials.[25]

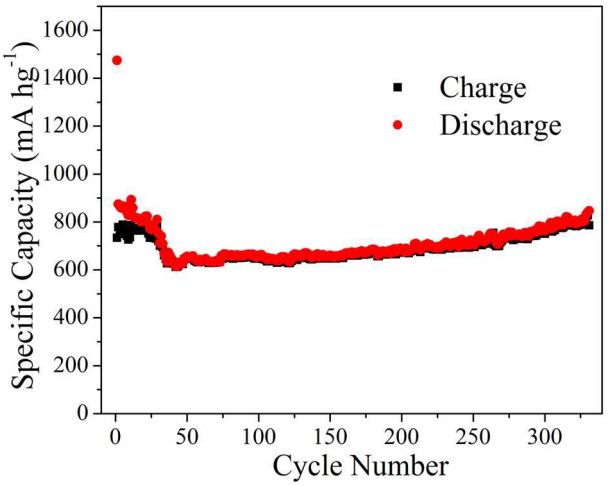

Figure 6. The long-term cycling performance of the $Ca_2Ge_7O_{16}$ nanowires/graphene sheets nanocomposite electrode under the current density of 500 mA g^{-1} and the voltage window of 0-3 V conditions.

To verify the long-term cyclability, the $Ca_2Ge_7O_{16}$ nanowires/graphene sheets nanocomposite anodes were further cycled between 0 and 3 V under the current density of 500 mA g^{-1}. **Figure 6** shows the specific capacity-cycle number curve, and it can be seen that the specific capacity decreased slightly before 50 cycles possibly owing to the polarization of the electode and after that the capacity began to increase step by step up to ca. 330 cycles possibly because of the slow activication process. Furthermore, it can be clearly seen that the least specific capacity is ca. 600 mA h g^{-1}, and the highest capacity can reach 800 mA h g^{-1} during the long-term cycle process. Such superior lithium storage performance further demonstrates the $Ca_2Ge_7O_{16}$ nanowires/graphene sheets nanocomposite can replace the conventional graphite to be the anodes for the next generation LIBs.

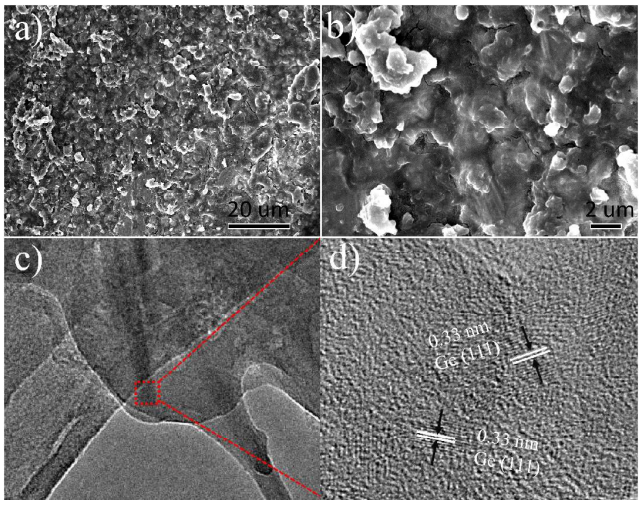

Figure 7. (a, b) The FESEM images; (c) TEM image (d) HRTEM image of the hybrid $Ca_2Ge_7O_{16}$ nanowires/graphene sheets electrode after 330 discharge/charge cycles at a current density of 500 mA g^{-1}.

To demonstrate the integrity of the $Ca_2Ge_7O_{16}$ nanowires/graphene sheets nanocomposite, the cell was disassembled after 330 cycles and investigated. As shown in Figure S7, it can be seen clearly that nanocomposite electrode

remained unchanged due to wrapping graphene buffering Ge volume change. And the electrode microstructure was further characterized by FESEM. As shown in **Figure 7a**, the $Ca_2Ge_7O_{16}$ nanowires/graphene sheets nanocomposite anode can remain free from electrode pulverization and exfoliation off the current collector. The enlarged image is shown in **Figure 7b**, and it can be seen that the nanowires or nanoparticles are highly uniform dispersed into the highly conductive and highly flexible mixed matrix, which can effectively adjust the volume expansion during cycling. The structural stability can be further proved by the TEM observation. **Figure 7c and 7d** represents a typical TEM image and its HRTEM image taken on the fully delithiated $Ca_2Ge_7O_{16}$ nanowires/graphene nanocomposite anode (red rectangular) after cycling 330 cycles, respectively. As shown in Figure 7c, The skeleton of $Ca_2Ge_7O_{16}$ nanowires is still retained after 330 cycles and the corresponding EDX spectrum (Figure S8) indicates that Ca, Ge, and O elements are also distributed on the nanowires. And the other elements (Cu, P, F, S) derived from the copper grid or foil and the eleltrolyte. Further, a ordered 0.33 nm lattice spacing can also be observed (Figure 7d) which is consistent with the (111) plane of *in-situ* formed intrinsic lithium-reactive Ge nanoparticles from germanate ($Ca_2Ge_7O_{16}$). These small Ge nano particles are highly uniform distributed in the mixture matrix of Li_2O, CaO and graphene that is favorable for both buffering the Ge volume change during lithiation/ delithiation and improving the conductivity of the whole electrode.

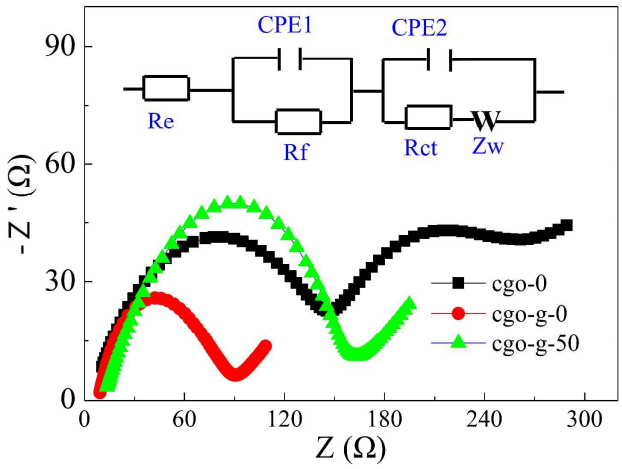

Figure 8. Electrochemical impedance spectra of the fresh $Ca_2Ge_7O_{16}$ anode (cgo-0) and $Ca_2Ge_7O_{16}$ nanowires/graphene sheets hybrid electrodes (fresh: cgo-g-0; after 50 cycles: cgo-g-50) obtained by applying a sine wave with amplitude of 5.0 mV over the frequency ranging from 100 kHz to 100 mHz.

To obtain further insight into such good electrochemical lithium storage performance of $Ca_2Ge_7O_{16}$ nanowires/graphene sheets nanocomposite, electrochemical impedance spectroscopy (EIS) measurements were performed (**Figure 8**). The equivalent model circuit of the system is also shown in the inset of Figure 8 to represent the internal resistance of the test anodes according to literature.[51-54] Re is the electrolyte resistance, the high-frequency semicircle corresponds to the contact resistance (R_f) and constant phase element of the SEI film formed on the anodes (CPE1), the semicircle in the medium-frequency region is assigned to the charge-transfer impedance (Rct) and constant phase element of electrode/electrolyte interface (CPE2), and Zw is associated with the Warburg impedance corresponding to the lithium ion diffusion into the anodes.[55] Obviously, the diameters of the semicircles for both fresh (cgo-g-0) and after 50 cycles (cgo-g-50 shown in Figure S9) $Ca_2Ge_7O_{16}$ nanowires/graphene sheets nanocomposite anode in the high-medium frequency region are much smaller than those of $Ca_2Ge_7O_{16}$ anode, respectively, revealing that the $Ca_2Ge_7O_{16}$ nanowires/graphene sheets nanocomposite anode owns lower contact and charge-transfer impedances. This result further validates that the encapsulating graphene can enhance the electrical conductivity of the overall electrode. In addition, from the low frequency inclined line, it can be found that the lithium-diffusion in the $Ca_2Ge_7O_{16}$ nanowires/graphene sheets anode is much easier than that in the $Ca_2Ge_7O_{16}$ anode, further confirming that the encapsulating graphene benefits the lithium-diffusion in the composite anode. The kinetic difference between $Ca_2Ge_7O_{16}$ and $Ca_2Ge_7O_{16}$ nanowires/graphene sheets anodes were further investigated by modeling AC EIS based on the modified equivalent circuit. The fitted parameters (Rf and Rct) of EIS are listed in Table 1. From the table, it can be clearly seen that the SEI film resistance (Rf) and charge-transfer resistance (Rct) of the $Ca_2Ge_7O_{16}$ nanowires/graphene sheets nanocomposite anode are 31.9 Ω and 46.02 Ω, respectively, which are significantly lower than those of the pristine $Ca_2Ge_7O_{16}$ nanowires anode (147.3 Ω and 80.6 Ω). And thus the value of exchange current density of nanocomposite anode is much larger than that of $Ca_2Ge_7O_{16}$ anode, indicating that the electro-chemical activity of the $Ca_2Ge_7O_{16}$ nanowires/graphene sheets nanocomposite anode is much higher than that of $Ca_2Ge_7O_{16}$ anode. This is favorable for anode material operation at high current density. This result once again confirms that the introduction of graphene can preserve the high conductivity of the $Ca_2Ge_7O_{16}$ nanowires/graphene sheets nanocomposite anode and greatly improve electron transport during the electrochemical lithium insertion/extraction reaction, resulting in significant improvement in the electrochemical performances. For the $Ca_2Ge_7O_{16}$ nanowires/graphene sheets nanocomposite anode, the diameter of the high-frequency semicircle increased to 89.15 Ω from 31.9 Ω (for the fresh anode) after the 50th cycle, which is explained that the SEI film on the surface of the anode grows thicker with cycle process. And this forming stable SEI film benefits the long-term cycling stability.[55] On the contrary, the charge-transfer impedance (Rct) (46.02 Ω for the fresh anode and 52.02 Ω for the 50th cycle) and the low-frequency related to the diffusion of lithium ions remain almost unchanged, indicating charge (e^- and Li^+) transportation remained fluent during cycling all the time.

Table 1: EIS parameters of the above-mentioned equivalent model circuit for the pristine $Ca_2Ge_7O_{16}$ nanowires and $Ca_2Ge_7O_{16}$ nanowires/graphene sheets nanocomposite anodes.

anodes	Rf	Rct
cgo-0	147.3	80.6
cgo-g-0	31.9	46.02
cgo-g-50	89.15	52.02

The enhanced cycle performance could be attributed to the following factors.

(1) Graphene, as a layered host with sp^2 carbon atoms, is used as a building block to wrap $Ca_2Ge_7O_{16}$ nanowires. Such structure not only offers a two dimensional high-express channel for Li^+, but also enhances the electrical conductivity of the anodes. Graphene encapsulating high-crystalline $Ca_2Ge_7O_{16}$ nanowires could enhance the conductivity greatly and dramatically decrease the Ohmic energy loss because of enhanced e^- transportation ability.

(2) The highly-crystalline $Ca_2Ge_7O_{16}$ nanowires with a diameter of ca. 10 nm could be tightly encapsulated into graphene sheets benefiting from *in-situ* hydrothermal route, which can guarantee a shorter Li^+ diffusion distance and large interfacial contact areas with the electrolytes. The thin thickness of graphene sheets and small crystal diameter of $Ca_2Ge_7O_{16}$ nanowires in $Ca_2Ge_7O_{16}$ nanowires/graphene sheets nanocomposite could significantly facilitate the liquid electrolyte to pass through the surface, so that more surface active sites would be created for Li^+.

(3) After the initial several cycles, the *in-situ* formed active Ge nanoparticles are highly dispersed within the mixed matrix of lithium-inert Li_2O, CaO and highly flexible graphene sheets, which not only provides an elastic buffer to accommodate the volume changes to protect the anodes from pulverization and exfoliation off the current collector to ensure every nanowire can actively participate in the electrochemical reaction, but also prevents the agglomeration of nanosized Ge particles during cycling.

(4) The enhanced lithium storage performance can result from the interconnectted two-dimensional conductive texture composed of the highly flexible, highly conductive and highly robust graphene sheets that not only act as the two-dimensional fluent conductive channels but also prevent volume expansion and the aggregation of Ge during cycling.

Conclusion

In summary, we have successfully developed a facile and efficient *in-situ* synthesis route for $Ca_2Ge_7O_{16}$ nanowires/graphene sheets nanocomposite. These unprecedented nanohybrids are composed of $Ca_2Ge_7O_{16}$ nanowires (diameter: ca. 10 nm) that are well-encapsulated and electronically assembled within 3D interconnecting frameworks of conducting graphene sheets. The results show that the as-prepared $Ca_2Ge_7O_{16}$ nanowires/graphene sheets nanocomposite exhibits highly reversible capacity, excellent cyclability, and superior rate capability as anodes of LIBs. This enhanced electrochemical lithium-storage performance may be assigned to the synergistic effect of the unique nanostructured hybrid, in which the $Ca_2Ge_7O_{16}$ nanowires are well-stabilized by the high conduction and flexibility of the graphene sheets. In addition, we envision that the other ternary compounds can be also encapsulated within graphene sheets in this facile way and applied in many other fields.

Acknowledgement

This work was supported by the National Natural Science Foundation (61377033).

Notes and references

[a] *School of Mathematics and Physics, University of Science and Technology Beijing (USTB), Beijing 100083, China. E-mail: chendi@ustb.edu.cn.*

[b] *Wuhan National Laboratory for Optoelectronics, Huazhong University of Science and Technology, Wuhan 430074, China.*

[c] *State Key Laboratory for Superlattices and Microstructures, Institute of Semiconductors, Chinese Academy of Sciences, Beijing 100083, China. E-mail: gzshen@semi.ac.cn.*

1 C. K. Chan, H. Peng, G. Liu, K. McIlwrath, X. F. Zhang, R. A. Huggins, Y. Cui, *Nat. Nanotechnol*., 2008, **3**, 31-35.
2 Z. Y. Wang, Z. C. Wang, S. Madhavi, X. W.(David) Lou, *Chem. Eur. J.*, 2012, **18**, 7561-7567.
3 X. Zhou, Y. X. Yin, L.-J. Wan, Y.-G. Guo, *Chem. Commun.*, 2012, **48**, 2198-2200.
4 G. Cui, L. Gu, L. J. Zhi, N. Kaskhedikar, P. A. van Aken, K. Müllen and J. Maier, *Adv. Mater.*, 2008, **20**, 3079.
5 Z. Y. Wang, Z. C. Wang, S. Madhavi, X. W. (David) Lou, *Chem. Eur. J.*, 2012, **18**, 7561-7567.
6 W. Li, X. Wang, B. Liu, S. Luo, Z. Liu, X. Hou, Q. Xiang, D. Chen, G. Shen, *Chem. Eur. J.*, 2013, **19**, 8650-8656.
7 D. Deng, J. Y. Lee, *Angew. Chem. Int. Ed.*, 2009, **48**, 1660-1663.
8 M. H. Park, Y. Cho, K. Kim, J. Kim, M. Liu, J. Cho, *Angew. Chem. Int. Ed.*, 2011, **50**, 9647-9650.
9 M. H. Park, Y. Cho, K. Kim, J. Kim, M. Liu, J. Cho, *Angew. Chem. Int. Ed.*, 2011, **50**, 9647-9650.
10 K. H. Seng, M. H. Park, Z. P. Guo, H. K. Liu, J. Cho, *Angew. Chem. Int. Ed.*, 2012, **124**, 5755-5759.
11 F. W. Yuan, H. J. Yang, and H. Y. Tuan, *ACS Nano*, 2012, **6**, 9932-9942.
12 D. J. Xue, S. Xin, Y. Yan, K. C. Jiang, Y. X. Yin, Y. G. Guo, L. J. Wan, *J. Am. Chem. Soc.*, 2012, **134**, 2512-2515.
13 C. S. Fuller, J. C. Severiens, *Phys. Rev.*, 1954, **96**, 21-24.
14 X. Li, Z. Yang, Y. Fu, L. Qiao, D. Li, H. Yue, D. He, *ACS Nano*, 2015, **9**, 1858-1867.
15 C. Zhang, Z. Lin, Z. Yang, D. Xiao, P. Hu, H. Xu, Y. Duan, S. Pang, L. Gu, G. Cui, *Chem. Mater.*, 2015, **27**, 2189-2194.
16 T. Kennedy, E. Mullane, H. Geaney, M. Osiak, C. O'Dwyer, K. M. Ryan, *Nano Lett.*, 2014, **14**, 716-723.
17 J. Hwang, C. Jo, M. G. Kim, J. Chun, E. Lim, S. Kim, S. Jeong, Y. Kim, J. Lee, *ACS Nano*, 2015, **9**, 5299-5309.
18 J. Liang, X. Li, Z. Hou, T. Zhang, Y. Zhu, X. Yan, Y. Qian, *Chem. Mater.* DOI: 10.1021/acs.chemmater.5b01527.
19 W. Tang, Y. Liu, C. Peng, M. Y. Hu, X. Deng, M. Lin, J. Z. Hu, K. P. Loh, *J. Am. Chem. Soc.* 2015, **137**, 2600-2607.
20 W. Li, M. Li, Z. Yang, J. Xu, X. Zhong, J. Wang, L. Zeng, X. Liu, Y. Jiang, X. Wei, L. Gu, Y. Yu, *Small*, DOI: 10.1002/smll.201403533.
21 X. Gao, W. Luo, C. Zhong, D. Wexler, S. Chou, H. Liu, Z. Shi, G. Chen, K. Ozawa, J. Wang, *Sci. Rep.* **4**, 6095.
22 X. Liu, J. Hao, X. Liu, C. Chi, N. Li, F. Endres, Y. Zhang, Y. Li, J. Zhao, *Chem. Commun.*, 2015, **51**, 2064-2067.
23 M. H. Park, K. Kim, J. Kim, J. Cho, *Adv. Mater.*, 2010, **22**, 415-418.
24 J. K. Feng, H. Xia, M. O. Lai, L. Lu, *J. Phys. Chem. C,* 2009, **113**, 20514-20520.
25 W. Li, Y. Yin, S. Xin, W. Song, Y. Guo, *Energy Environ. Sci.*, 2012, **5**, 8007-8013.
26 F. Zou, X. Hu, Y. Sun, W. Luo, F. Xia, L. Qie, Y. Jiang, Y. Huang, *Chem. Eur. J.*, 2013, **19**, 6027-6033.
27 S. Wu, R. Wang, Z. Wang, Z. Lin, *Nanoscale*, 2014, **6**, 8350-8358.
28 S. Jin, C. Wang, *Nano Energy*, 2014, **7**, 63-71.
29 R. Yi, J. K. Feng, D. P. Lv, M. Gordin, S. R. Chen, D. Choi, D. H. Wang, *Nano Energy*, 2013, **2**, 498-504.
30 C. H. Kim, Y. S. Jung, K. T. Lee, J. H. Ku, S. M. Oh, *Electrochim. Acta*, 2009, **54**, 4371-4377.
31 D. Li, C. Feng, H. Liu, Z. Guo, *Sci. Rep.* 2015, **5**, 11326.
32 T. Lv, X. Li, J. Ma, *RSC Adv*., 2014, **4**, 49942-49945.
33 H. L. Yu, C. Ma, B. H. Ge, Y. J. Chen, Z. Xu, C. L. Zhu, C. Y. Li, Q. Y. Ouyang, P. Gao, J. Q. Li, C. W. Sun, L. H. Qi, Y. M. Wang, F. H. Li, *Chem. Eur. J.*, 2013, **19**, 5818-5823.
34 Y. M. Wu, Z. H. Wen, H. B. Feng, J. H. Li, *Chem. Eur. J.* 2013, 19, 5631-5636.

35 J. Ha, S. Park, S. Yu, A. Jin, B. Jang, S. Bong, I. Kim,Y. Sung, Y. Piao, *Nanoscale*, 2013, **5**, 8647-8655.

36 J. Yang, J. Wang, Y. Tang, D. Wang, X. Li, Y. Hu, R. Li, G. Liang, T. Sham, X. Sun, *Energy Environ. Sci*., 2013, **6**, 1521-1528.

37 Y. Wen, Y. J. Zhu, A. Langrock, A. Manivannan, S. H. Ehrman, C. S. Wang, *Small*, 2013, **9**, 2810-2816.

38 A. C. Ferrari, J. Robertson, *Phys. Rev. B*, 2000, **61**, 14095-14107.

39 J. K. Feng, M. O. Lai, L. Lu, *Electrochem. Commun.*, 2011, **13**, 287-289.

40 J. Graetz, C. C. Ahn, R. Yazami, B. Fultz, *J. Electrochem. Soc.*, 2004, **151**, A698-A702.

41 K. H. Seng, M. Park, Z. P. Guo, H. Liu, J. Cho, *Nano Lett.*, 2013, **13**, 1230-1236.

42 F. Zou, X. Hu, L. Qie, Y. Jiang, X. Xiong, Y. Qiao, Y. Huang, *Nanoscale*, 2014, **6**, 924-930.

43 Z. Chen, Y. Yan, S. Xin, W. Li, J. Qu, Y. Guo, W. Song, *J. Mater. Chem. A*, 2013, **1**, 11404-11409.

44 W. Li, X. Wang, B. Liu, J. Xu, B. Liang, T. Luo, S. Luo, D. Chen, G. Shen, *Nanoscale*, 2013, **5**, 10291-10299.

45 Z. Y. Wang, Z. C. Wang, W. T. Liu, W. Xiao, X. W. Lou (David), *Energy Environ. Sci.*, 2013, **6**, 87-91.

46 S. J. Ding, Z. Y. Wang, S. Madhavi, X. W.(David) Lou, *J. Mater. Chem.*, 2011, **21**, 13860-13864.

47 Y. S. Luo, J. S. Luo, J. Jiang, W. W. Zhou, H. P. Yang, X. Y. Qi, H. Zhang, H. J. Fan, D. Y. W. Yu, C. M. Li, T. Yu, *Energy Environ. Sci.*, 2012, **5**, 6559-6566.

48 G. Lee, J. Kim, D. Lee, S. Seo, H. Shim, D. Kim, *Chemelectrochem*, 2014, **3**, 673-678.

49 J. S. Chen, X. W. Lou (David), *Small*, 2013, **9**, 1877-1893.

50 M. H. Seo, M. Park, K. T. Lee, K. Kim, J. Kim, J. Cho, *Energy Environ. Sci.*, 2011, **4**, 425.

51 S. Yang, X. Feng, S. Ivanovici, K. Müllen, *Angew. Chem. Int. Ed.* 2010, **49**, 8408-8411.

52 K. Chang, W. X. Chen, *ACS Nano*, 2011, **28**, 4720-4728.

53 P. Guo, H. Song, X. Chen, *Electrochem. Commun.* 2009, **11**, 1320-1324.

54 H. Liu, G. Wang, J. Wang, D. Wexler, *Electrochem. Commun.* 2008, **10**, 1879-1882.

55 S. Yang, H. Song, X. Chen, *Electrochem. Commun.*, 2006, **8** 137-142.